

Locomotion-Action-Manipulation: Synthesizing Human-Scene Interactions in Complex 3D Environments

Jiye Lee Hanbyul Joo
Seoul National University
{kay2353, hbjoo}@snu.ac.kr

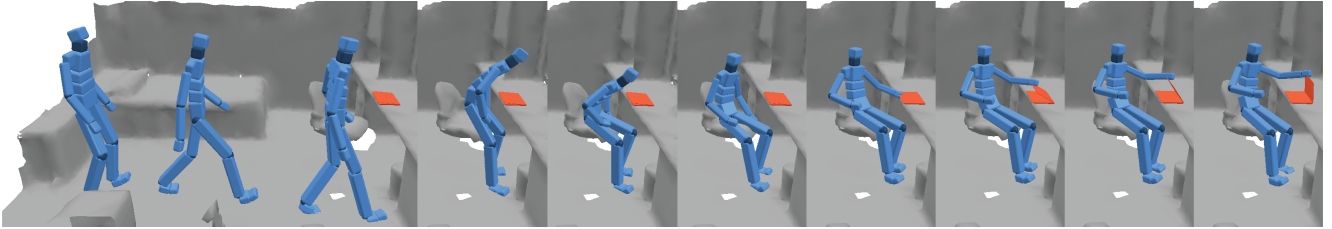


Figure 1. Our system, LAMA, produces high-quality and realistic 3D human motions that include locomotion, scene interactions, and manipulations given a 3D environment and designated interaction cues.

Abstract

Synthesizing interaction-involved human motions has been challenging due to the high complexity of 3D environments and the diversity of possible human behaviors within. We present LAMA, Locomotion-Action-MANipulation, to synthesize natural and plausible long term human movements in complex indoor environments. The key motivation of LAMA is to build a unified framework to encompass a series of motions commonly observable in our daily lives, including locomotion, interactions with 3D scenes, and manipulations of 3D objects. LAMA is based on a reinforcement learning framework coupled with a motion matching algorithm to synthesize locomotion and scene interaction seamlessly under common constraints and collision avoidance handling. LAMA also exploits a motion editing framework via manifold learning to cover possible variations in interaction and manipulation motions. We quantitatively and qualitatively demonstrate that LAMA outperforms existing approaches in various challenging scenarios. Project page: <https://lama-www.github.io/>.

1. Introduction

In our daily lives, we can easily observe that humans do not live in isolation nor in voids, but continuously interact with a complex environment surrounded by many objects.

Notably, humans perform such a diverse set of daily life actions effortlessly. Imagine that we visit a new indoor environment (e.g., a hotel room) we have never been before. It is expected that we can still easily figure out how to move from rooms to rooms, how to sit on a chair, how to open the doors of closets, and so on. However, endowing machines or virtual humans with such abilities is still a largely unexplored area, despite its importance.

Synthesizing scene interactions within real-life 3D environments has been a challenging research problem due to its complexity and diversity. Human movements in real life consists of various types of behaviors, including locomotion with avoiding cluttered areas, diverse interactions with 3D scenes, and sophisticated object-manipulations. In particular, the spatial constraint that arises from real-life 3D environments where many objects are cluttered makes motion synthesis highly constrained and complex, and various possible arrangements of 3D environments make generalization difficult. As human-scene interactions cover a wide range of technical challenges, previous approaches have focused on sub-problems, such as (1) modeling static poses [17, 24, 49, 64, 69, 71, 72] or (2) human object interactions with a single target object or interaction type [10, 47, 53–55, 66, 67, 70]. Recent methods [15, 59, 60] extend to synthesizing dynamic interaction motions in cluttered real-world 3D scenes. However, the performance of these methods are fundamentally limited due to the lack of 3D ground truth data that contains both human motions and paired 3D environments.

In this paper, we present LAMA, **L**ocomotion-**A**ction-**M**anipulation, to synthesize natural and plausible long term human motions in complex indoor environments. The key motivation of LAMA is to build a unified framework to include locomotion, interactions with 3D scenes, and manipulations of 3D objects, which are the series of motions commonly observable in our daily lives. LAMA is based on a reinforcement learning framework coupled with a motion matching algorithm to synthesize locomotion and scene interaction seamlessly while adapting to complicated 3D scenes with collision avoidance handling. The reinforcement learning framework interprets the 3D information of the given scene and optimally traverses among the motion capture database via motion matching. As an advantage, our system does not require any “scene-paired” datasets where human movements are captured with the surrounding 3D environments simultaneously, which is rarely available. To further cover the numerous variations of interaction motions, we also exploit an autoencoder based motion editing approach to learn the motion manifold space [20] in which the editing is performed. Through extensive quantitative and qualitative evaluations against existing approaches, we demonstrate that our method outperforms previous methods in various challenging scenarios.

Our contributions are summarized as follows: (1) we present the first method to generate realistic long term motions combined with locomotion, interaction with scene, and manipulation in complicated cluttered scenes; (2) we propose a novel, unified framework that synthesizes locomotion and human-scene interactions in a seamless manner, by introducing scene interpretation terms to a reinforcement learning based approach to automatically generate optimal transitions; and (3) our outputs show the state-of-the-art motion synthesis quality with longer duration (more than 10 sec) than previous methods.

2. Related Work

Generating Human-Scene Interactions. Generating natural human motion has been a widely researched topic in the computer vision community. Early methods focus on synthesizing or predicting human movements by exploiting neural networks [11, 13, 35, 35, 38, 46, 56, 58]. However, these approaches primarily address the synthesis of human motion itself, without taking into account the surrounding 3D environments. Recent approaches begin to tackle modeling and synthesizing human interactions within 3D scenes, or with objects. Most of the researches focus on statically posing humans within the given 3D environment [16, 24, 69, 71], by generating human scene interaction poses from various types of input including object semantics [17], images [21, 23, 64, 65, 68], and text descriptions [49, 72].

More recently, there have been approaches to synthesize dynamic human object interactions (e.g., sitting on chairs,

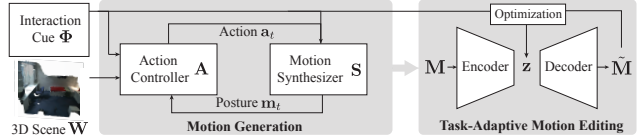


Figure 2. Overview of LAMA.

carrying boxes). Starke et al. [53] introduce an autoregressive learning framework with object geometry-based environmental encodings to synthesize various human-object interactions. Later work [15, 70] extends this by synthesizing motions conditioned with variations of objects and contact points. Other approaches [47, 54, 55, 66, 67] focus on generating natural hand movements for manipulation, which is extended by including full body motions [54]. Physics-based character control to synthesize human object interactions has been also explored in [8, 10, 39, 47, 66]. Although these approaches cover a wide range of human object interactions, most of them solely focus on the relationship between human and the target object without long-term navigation in cluttered 3D scenes.

More recent approaches include generating natural human scene interactions within a complex 3D scene cluttered with many objects [6, 59–61], closely related to ours. These methods are trained using human motion datasets paired with 3D scenes, which require both ground truth motions and simultaneously captured 3D scenes for supervision. Due to such difficulties, some methods exploit synthetic datasets [6, 61] or data fitted from depth videos [60]. In previous approaches [15, 59], navigation to move through cluttered environments is often performed by a separate module via a path planning algorithm (e.g., A^* algorithm) by approximating the volume of a human as a cylinder. This path planning based methods approximate the spatial information of the scene and the human body and therefore have limitations under highly complex conditions.

Motion Synthesis and Editing. Synthesizing natural human motions by leveraging motion capture data has also been a long-researched topic in computer graphics. Some approaches [26, 37] construct motion graphs, where plausible transitions are inserted as edges and motion synthesis is done by traversing through the constructed graph. Similar approaches [31, 51] connect motion patches to synthesize interactions in a virtual environment or multi-person interactions. Due to its versatility and simplicity, a number of variations have been made on the graph based approach, such as motion grammar [22] which enforces traversing rules in the motion graph. Motion matching [5, 9] can also be understood as a special case of motion graph traversal, where the plausible transitions are not precomputed but searched during runtime. Recent advances in deep learning allow to leverage motion capture data for motion manifold

learning [19, 20, 52]. Autoregressive approaches based on variational autoencoders (VAE) [36, 46] and recurrent neural networks [14, 29, 41] are also used to forecast future motions based on past frames. These frameworks are generalized to synthesizing a diverse set of motions including locomotion on terrains [19] mazes [36], action-specified motions [46], and interaction-involved sports [29, 41]. Neural network-based methods are also reported to be successful in various motion editing tasks such as skeleton retargeting [2], style transfer [3, 20], and inbetweening [14].

Reinforcement learning (RL) has also been successful in combination with both data-driven and physics-based approaches for synthesizing human motions. Combined with data-driven approaches, these RL frameworks serve as a control module that generates corresponding motions to a given user input by traversing through motion graphs [28], latent space [34, 36, 57], and precomputed transition tables [30]. Deep reinforcement learning (DRL) has been widely used recently in physics simulation as well to synthesize physically plausible movements with a diverse set of motor skills [4, 32, 41, 43–45, 62].

3. Method

3.1. Overview

Our system, dubbed as *LAMA*, outputs a sequence of human poses $\mathbf{M} = \{\mathbf{m}_t\}_{t=1}^T$ by taking the 3D surrounding cues \mathbf{W} and desired interaction cues Φ , as inputs:

$$\mathbf{M} = \mathcal{LAMA}(\mathbf{W}, \Phi). \quad (1)$$

The output posture at time t , $\mathbf{m}_t = (p_0, r_1, \dots, r_J) \in \mathbb{R}^{3J+3}$, is represented by a concatenated vector of global root position $p_0 \in \mathbb{R}^3$ and local joint orientations of J joints where each j -th joint is in angle-axis representations $r_j \in so(3)$. Throughout our system, the skeleton tree structure and joint offsets are fixed and shown in Fig. 3 (a). We represent the 3D environments $\mathbf{W} = \{\mathbf{w}_i\}$ as a set of 3D object and environment meshes, including the background scene mesh and other object meshes targeted for manipulation. The interaction cues, $\Phi = [\phi_1, \phi_2, \dots, \phi_n]$, are an ordered list of desired interaction inputs $\phi_i = \{\mathbf{q}_j\}_{j \in J^i}$ where $\mathbf{q}_j \in \mathbb{R}^3$ indicates desired positions of j -th joint, and J^i is a set of specified joints for interaction (in practice, few joints such as root¹ or end-effectors). Examples of the 3D environment \mathbf{W} and interaction inputs ϕ_i are shown in Fig. 5 (a). Intuitively, ϕ_i specifies the expected positions of selected joints of the human character. Note that we do not specify the exact timing of the interaction, as the timing is automatically determined by our action controller. More details are addressed in Sec. 3.4.

To synthesize locomotion, interaction, and manipulation together, *LAMA* is designed via a three-level system com-

¹For root, orientation in angle-axis representation is also included in ϕ .

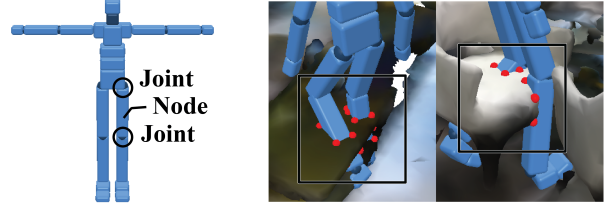


Figure 3. (a) Skeleton with joints and box nodes. (b) Automatically detected collision points (colored as red).

posed of the action controller \mathbf{A} and the motion synthesizer \mathbf{S} , followed by a manifold-based motion editor \mathbf{E} . By taking 3D scene cues \mathbf{W} and desired interaction cues Φ as input, the action controller \mathbf{A} makes the use of a reinforcement learning (RL) framework by training the control policy π to sample an action at time t , $\pi(\mathbf{a}_t | \mathbf{s}_t, \mathbf{W}, \Phi)$, where \mathbf{a}_t contains the plausible next action cues including predicted action types and short-term future forecasting. \mathbf{s}_t is the state cues to represent the current status of human characters including its body posture, surrounding scene occupancy, and current target interaction cue, which can be computed via a function ψ , $\mathbf{s}_t = \psi(\mathbf{m}_{t-1}, \mathbf{m}_t, \mathbf{W}, \Phi)$. Intuitively, action controller \mathbf{A} predicts the plausible next action cues \mathbf{a}_t by considering the current character-scene state \mathbf{s}_t . The generated action signals \mathbf{a}_t from the action controller \mathbf{A} is provided as the input for the motion synthesizer \mathbf{S} , which then determines the posture at the next time step \mathbf{m}_{t+1} , i.e., $\mathbf{S}(\mathbf{m}_t, \mathbf{a}_t) = \mathbf{m}_{t+1}$. Afterwards, the character’s next state can be computed again via $\mathbf{s}_{t+1} = \psi(\mathbf{m}_t, \mathbf{m}_{t+1}, \mathbf{W}, \Phi)$, which is input to the action controller recursively.

Followed by the initial motion generation part from \mathbf{A} and \mathbf{S} , our system furthermore applies a motion editor $\mathbf{E}(\mathbf{M}) = \tilde{\mathbf{M}}$, where $\tilde{\mathbf{M}} = \{\tilde{\mathbf{M}}_t\}_{t=1}^T$ is the edited motions to further express the motions involving complex human-object interactions such as manipulation (e.g. moving objects, opening doors). Fig. 2 shows the overview of *LAMA*.

3.2. Scene-Aware Action Controller

Based on reinforcement learning, our action controller \mathbf{A} enables the character to perform locomotion and desired actions with fulfilling the interaction cues Φ and avoiding collisions in the 3D environment \mathbf{W} . \mathbf{A} is a trained control policy π where $\pi(\mathbf{a}_t | \mathbf{s}_t, \mathbf{W}, \Phi)$. Different from previous approaches where navigation and scene-object interactions (e.g., sitting) are performed by separate modules [15, 59], our RL-based framework performs both in a unified way with a common objective by automatically determining the transition from navigation to specific actions. As a key advantage, *LAMA* can be robustly generalized to challenging unseen 3D clutters in long-term human motion synthesis and also outperforms previous methods by avoiding collisions throughout the whole process, including navigation

and interaction.

State. The state $\mathbf{s}_t = \psi(\mathbf{m}_{t-1}, \mathbf{m}_t, \mathbf{W}, \Phi)$ at time t is a feature vector representing the current status of the human character. $\mathbf{s}_t = (\mathbf{s}_t^{body}, \mathbf{s}_t^{scene}, \mathbf{s}_t^{inter})$ is composed of body configuration \mathbf{s}^{body} , 2D scene occupancy \mathbf{s}^{scene} , and desired current target interaction \mathbf{s}^{inter} . Body configuration $\mathbf{s}^{body} = \{r, \dot{r}, \theta_{up}, h, \mathbf{p}_e\}$ includes $r, \dot{r} \in \mathbb{R}^{J' \times 6}$ that are the joint rotations and velocities respectively for the J' joints excluding the root in 6D representations [73], $\theta_{up} \in \mathbb{R}$ that is the up vector of the root (represented by the angle w.r.t the Y-axis), $h \in \mathbb{R}$ that is the root height from the floor, and $\mathbf{p}_e \in \mathbb{R}^{e \times 3}$ that is the end-effector positions in person-centric coordinate (where e is the number of end-effectors). $\mathbf{s}^{scene} = \{\mathbf{g}_{occ}, \mathbf{g}_{root}\}$ includes scene occupancy information in 2D floor plane, as shown in Fig. 4. $\mathbf{g}_{occ} \in \mathbb{R}^{n^2}$ represents the 2D occupancy grid on the floor plane of neighboring n cells around the agent and $\mathbf{g}_{root} \in \mathbb{R}^2$ denote the current 2D global root position of the character in the discretized grid plane. \mathbf{s}^{inter} is an element of Φ and represents the interaction cue the character is currently targeting, that is $\mathbf{s}^{inter} = \phi_i$.

Action. Given the current status of the character \mathbf{s}_t , the control policy π outputs the feasible action $\mathbf{a}_t = (\mathbf{a}_t^{type}, \mathbf{a}_t^{future}, \mathbf{a}_t^{offset})$. \mathbf{a}_t^{type} provides the probabilities of next action type among all possible actions, determining the transition timing between actions (e.g., from locomotion to sitting). \mathbf{a}_t^{future} predict future motion cues such as plausible root position for the next 10, 20, and 30 frames. \mathbf{a}_t^{offset} is intended to update the raw motion data searched from the motion database in motion synthesizer module **S**. Intuitively, our learned control policy generates an optimal posture offset \mathbf{a}_t^{offset} which is applied to the closest plausible raw posture in the database. This enables the character to perform more plausible scene-aware human poses, allowing our system to be generalized to any unseen 3D scenes given a limited amount of motion capture data. More details are addressed in Sec. 3.3.

3.3. Motion Synthesizer

Given the current motion output \mathbf{m}_t and actions signals \mathbf{a}_t from the action controller **A** as inputs, the motion synthesizer produces the next plausible character posture: $\mathbf{S}(\mathbf{m}_t, \mathbf{a}_t) = \mathbf{m}_{t+1}$. As the first step, motion synthesizer searches for the motion from a motion database that best matches the closest motion feature, then modifies the searched raw motion to be more suitable for the scene environment. To this end, motion synthesizer’s output \mathbf{m}_{t+1} is in turn fed into the action controller recursively. We exploit a modified version of motion matching algorithm [5, 9, 18] for the first step of motion synthesis. In motion matching, motion synthesis is performed periodically by searching the most plausible next shot motion segments from a motion DB, and compositing them into a long connected sequence.

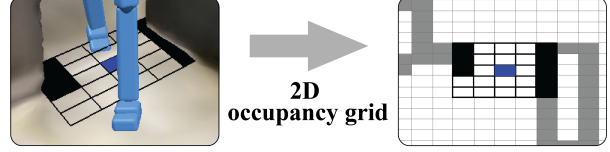


Figure 4. Visual representation of the 2D occupancy grid near the root. Grid on the right represents top view of the grid. Blue indicates root position while gray represents the space is occupied. Occupied cells near the root are colored as black.

Motion features. Motion feature represents the characteristic of each frame in the short motion segment and is computed as $f(\mathbf{m}) = \{\{p_j\}, \{\dot{p}_j\}, \theta_{up}, c, \mathbf{o}_{future}\}$. From a posture \mathbf{m} , the positions and velocities $p_j, \dot{p}_j \in \mathbb{R}^3$ are extracted for the selected joints $j \in \{\text{Head}, \text{Hand}, \text{Foot}\}$, which are defined in a person-centric coordinate of \mathbf{m} . $\theta_{up} \in \mathbb{R}^3$ is the up-vector of the root joint, and $c \in \{0, 0.5, 1\}$ indicates automatically computed foot contact cues of the left and right foot (0 for non-contact, 1 for contact, 0.5 for non-contact but close to the floor within a threshold). $\mathbf{o}_{future} = \{\{p_0^{dt}\}, \{r_0^{dt}\}\}$ contains the cues for the short-term future postures, where p_0^{dt} and r_0^{dt} are the position and orientation of root joint at dt frames later from the current target frame. \mathbf{o}_{future} are computed in 2D XZ plane in person-centric coordinate of the current target motion \mathbf{m} , and thus $p_0^{dt}, r_0^{dt} \in \mathbb{R}^2$. The selected future frames are action-type specific, and for locomotion we extract 10, 20, and 30 frames in the future (at 30Hz) following [9]. Intuitively, the motion feature extracts the target frame’s posture and temporal cues by considering neighboring frames². We pre-compute motion features for every frame of the motion clips in the motion database. Motion feature of the current state of the character, or the query feature, is also computed in the same way based on posture $\mathbf{m}_{t-1}, \mathbf{m}_t$ and \mathbf{a}_t^{future} produced by the action controller, that is $\mathbf{x}_t = f(\mathbf{m}_{t-1}, \mathbf{m}_t, \mathbf{a}_t^{type}, \mathbf{a}_t^{future})$. The component \mathbf{a}_t^{future} serves as \mathbf{o}_{future} in the query feature, which can be understood as the action controller providing cues for predicted future postures.

Motion searching and updating. The query motion feature \mathbf{x}_t from the current character is computed as addressed above, and let the motion features in motion database denoted as \mathbf{y}_k for the k -th clips in the DB. Motion searching finds the best matches in the motion database by computing the weighted euclidean distances between the query feature and DB features:

$$\mathbf{k}^* = \arg \min_k \|\mathbf{w}_f^T (\mathbf{x}_t - \mathbf{y}_k)\|^2, \quad (2)$$

where \mathbf{w}_f is a fixed weight vector to control the impor-

²In practice, the input of feature extractor function f should take into account the motions of neighboring timesteps.

tance of feature elements. After finding the best match $\hat{\mathbf{m}}_{k^*}$ from motion database, the motion synthesizer further updates it with the predicted motion offset \mathbf{a}_t^{offset} from \mathbf{a}_t , that is $\tau(\hat{\mathbf{m}}_{k^*+1}, \mathbf{a}_{offset}) = \mathbf{m}_{t+1}$, where $\hat{\mathbf{m}}_{k^*+1}$ is the next plausible character posture and τ is an update function to update selected joints. In practice, the motion searching is performed periodically (e.g., every N-th frames) to make the synthesized motion temporally more coherent.

3.4. Learning for Scene-Aware Action Controller

In the reinforcement learning framework, the objective is to learn the optimal policy which maximizes the discounted cumulative reward. In our method, we design rewards to guide the agent to perform locomotion towards the target objects (e.g., sofa) and also perform desired interaction with the object (e.g., sitting). In particular, our RL-framework performs both navigation and interaction with common constraints (e.g., smooth transitions, collision avoidance).

Our reward function consist of the following terms:

$$R_{total} = w_{tr}R_{tr} + w_{act}R_{act} + w_{reg}R_{reg}, \quad (3)$$

where w_{tr} , w_{act} , and w_{reg} are the weights to balance among reward terms. The trajectory reward R_{tr} is obtained when the character moves towards the desired interaction input ϕ while meeting the spatial constraints from the surrounding 3D scene, described below:

$$R_{tr} = r_{coli} \cdot r_{pos} \cdot r_{root}, \quad \text{where} \quad (4)$$

$$r_{coli} = \exp\left(-\frac{1}{\sigma_{coli}^2} \sum_{b \in \mathbf{B}} w_b \rho(b, \mathbf{W})\right), \quad (5)$$

$$r_{pos} = \exp\left(-\frac{1}{\sigma_{root}^2} \sum_{j \in \mathbf{J}} \|\mathbf{p}_0 - \mathbf{q}_j\|^2\right), \quad (6)$$

$$r_{vel} = \begin{cases} 1 & \text{when } \dot{\mathbf{p}}_{root} \geq \sigma_{th} \\ \sigma_{vel} \|\dot{\mathbf{p}}_0\|^2 & \text{else.} \end{cases} \quad (7)$$

The collision-avoidance reward r_{coli} penalizes collisions with 3D scenes. As depicted in Fig. 3 (a), body limbs in the skeletal structure are represented as a set of box-shaped nodes \mathbf{B} with a fixed width, where each element $b \in \mathbf{B}$ is a 3D box representation of legs and arms (we exclude torso and head). The function $\rho(b, \mathbf{W})$ detects the collision between edges of a box-shaped node b with 3D scene meshes \mathbf{W} and returns the number of intersection points. (Fig. 3 (b)). w_b is the weights to control importance of each limb b . The collision-avoidance reward is maximized when no penetration occurs, making the control policy π to find the optimal trajectory and pose offset to avoid physically implausible collisions and penetrations. r_{pos} are obtained when the agent moves to reach the targeting interaction cue ϕ , by encouraging agent’s root position p_0 to be closer to the target

interaction cue $\{\mathbf{q}_j\}$. r_{vel} encourages the character to move by penalizing when the root velocity $\dot{\mathbf{p}}_{root}$ is less than a threshold σ_{th} . σ_{coli} , σ_{root} , and σ_{vel} are weights to control the balance between terms.

Action reward R_{act} enforces the synthesized motion to fulfill the given interaction cue $\phi = \{\mathbf{q}_j\}$:

$$R_{act} = r_{inter} \cdot r_{\Delta t} \cdot r_{\Delta v}, \quad \text{where} \\ r_{inter} = \exp\left(-\frac{1}{\sigma_{inter}^2} \sum_{j \in \mathbf{J}} \|\mathbf{p}_j - \mathbf{q}_j\|^2\right), \quad (8) \\ r_{\Delta t} = \exp(-\sigma_{\Delta t}^2 C_{tr}), \\ r_{\Delta v} = \exp(-\sigma_{\Delta v}^2 C_{vel}),$$

where interaction reward term r_{inter} is maximized when the performed action meets the positional constraints provided by interaction cues. Smoothness reward terms $r_{\Delta t}$ and $r_{\Delta v}$ minimizes the transition cost, which is based on the subpart of the feature distances defined in Eq. 2, where C_{tr} is the weighted feature distances of p_j , θ_{up} , and c , and C_{vel} is from \dot{p} . These are intended to penalize the case where the character makes abrupt changes.

Regularization reward R_{reg} penalizes the \mathbf{a}_t^{offset} excessively modifying the original posture brought from the motion synthesizer, denoted as $\hat{\mathbf{m}}_t$, and maintains temporal consistency among frames.

$$R_{reg} = \exp\left(-\frac{1}{\sigma_{reg}^2} \left(\|\hat{\mathbf{m}}_t - \mathbf{m}_t\|^2 + \|\mathbf{m}_t - \mathbf{m}_{t-1}\|^2\right)\right).$$

It is reported that [33, 41] multiplying rewards with consistent goals are suitable for learning, as the reward is received when the conditions are simultaneously met. Furthermore, to accelerate learning, we use early termination conditions [43] and limited action transitions. The episode is terminated when the character moves out of the scene bounding box, or when the collision reward r_{coli} is under a certain threshold. Also, the action controller first checks in advance whether the action signal is valid when it makes transitions from locomotion to other actions. When the nearest feature distance of Eq. 2 in the motion synthesizer is over a certain threshold, the action controller discards the transition and continues navigating. The control policy is learned through Proximal Policy Optimization (PPO) algorithm [50].

3.5. Task-Adaptive Motion Editing

Interaction includes a massively diverse pool of motions, and these variations cannot be fully handled by limited amount of motion database. In order to cover such diversity, we include a task-adaptive motion editing module in our motion synthesis framework. The goal of our editing module \mathbf{E} is (1) to edit motion \mathbf{M} to fit into diverse

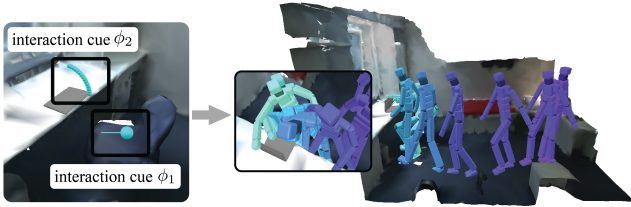


Figure 5. Visual representation of system input Φ , \mathbf{W} and output motion sequence. On the left, interaction cues are shown as cyan spheres and arrows (indicating orientation). The right is the synthesized human motion $\tilde{\mathbf{M}}$.

target object geometries (e.g., sitting on a chair with different height), and (2) to generate additional hand movements for manipulation (e.g., grasping). In particular, in the case of manipulation, additional interaction cue ϕ can be provided to enforce an end-effector (e.g., a hand) to follow the desired trajectories to express the manipulation task on the target object, as shown in Fig 8 (left). The edited motion $\tilde{\mathbf{M}} = E(\mathbf{M})$ should not only fulfill the sparsely given positional constraints, but also preserve the temporal consistency between frames and spatial correlations among joints in order to maintain its naturalness. We adopt the motion manifold learning approach with convolutional autoencoders [20] to compress motion to a latent vector within a motion manifold space. Motion editing is done by searching for an optimal latent vector among the manifold. For training the autoencoder, motion sequence, which we denote as \mathbf{X} converted from \mathbf{M} , is represented as a time-series of human postures by concatenating joint rotations in 6D representations [73], root height, root transform relative to the previous frame projected on the XZ plane, and foot contact labels. The encoder and decoder module are trained based on reconstruction loss, $\|\mathbf{X} - \Psi^{-1}(\Psi(\mathbf{X}))\|^2$, where Ψ is the encoder and Ψ^{-1} is the decoder.

The latent vector from the encoder $\mathbf{z} = \Psi(\mathbf{X})$ represent the motion manifold space by preserving the spatio-temporal relationship among joints and frames within the motion sequence. As demonstrated in [20], editing motions in this manifold space ensures the edited motion to be realistic and temporally coherent. To this end, we find the optimal latent vector \mathbf{z}^* by minimizing a loss function \mathcal{L} by constraining the outputs motions to follow the interaction constraint ϕ . We also include additional regularizers in \mathcal{L} so that the output motion to maintain the foot locations and root trajectories to the original motions. See supp. mat. for more details on \mathcal{L} . Finally, the edited motion $\tilde{\mathbf{M}}$ can be computed via $\Psi^{-1}(\mathbf{z}^*)$.

4. Experiments

We evaluate LAMA’s ability on synthesizing long-term motions with various human-scene and human-object inter-

Method	Plausibility		Naturalness		
	Slip	Penetration	FD _{total}	FD _{root}	FD _{joint}
Wang et al. [60]	5.13	3.88	1.38	0.45	0.93
Wang et al. [60]*	24.8	4.58	1.44	0.44	1.00
SAMP [15]	10.5	12.49	1.25	0.30	0.95
LAMA (ours)	5.21	1.52	1.22	0.31	0.91

Table 1. **Baseline comparison** Foot slip loss (cm, ↓) averaged over all frames. Penetration loss(percentage, ↓) is counted based on intersection points of the 3D environment and the skeleton. Naturalness score is based on fréchet distance (FD ↓). Wang et al. with an asterisk indicates without post-processing optimization.

actions involved. We exploit an extensive set of quantitative metrics and perceptual study to evaluate the physical plausibility and naturalness of the synthesized motion.

Dataset. For constructing the database for the motion synthesizer, motion capture data are selectively collected and refined from Ubisoft La Forge [14], COUCH [70], and SAMP [15]. All the data used in this system are motion capture data (in bvh format) with no scene or object related information, and are retargeted into a unified skeletal structure with MotionBuilder. We use PROX [16] and Matterport3D [7] datasets for 3D environment and SAPIEN [63] object meshes for manipulation. Our code and pre-processed data will be publicly released.

Implementation Details. The policy and the value network of the action controller module consists of 4 and 2 fully connected layers of 256 nodes, respectively. The encoder and decoder of the task-adaptive motion editing module consist of three convolutional layers. Adam optimizer [25] is used for training and optimization. We use Nvidia RTX 3090 for training the action controller and the motion editing module. It takes 10 to 80 minutes to learn a single control policy, where the training time mainly depends on how difficult the interaction cues are to achieve. For optimization in the motion editing module, it takes 3 to 4 minutes for 500 epochs. See supp. mat. for more detail.

4.1. Experimental Setup

Evaluation metrics. Quantifying motion synthesis quality is challenging due to the lack of ground-truth data or official evaluation metrics. We try to quantify them in terms of physical plausibility and naturalness.

- **Physical plausibility:** We use contact and penetration metrics to evaluate the physical plausibility of the synthesized motions. Contact loss penalizes the foot movement when the foot is in contact. Since foot contact is a critical element in dynamics, contact-based metric is closely related in determining the physical plausibility of motions. Penetration loss (“Penetration” in Table 1) measures implausible cases when the body penetrates the objects in the scene. We compute penetration metric by counting frames where the

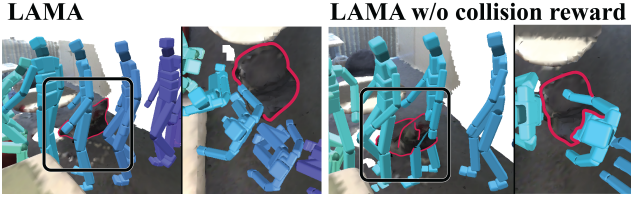


Figure 6. Comparison with LAMA (left) and LAMA without collision reward (right). As shown in the right, without collision reward the character fails to avoid collisions with obstacles (marked as red).

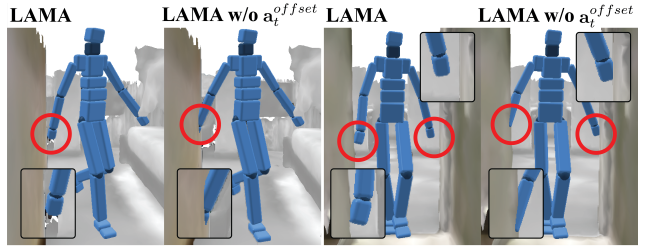


Figure 7. Comparison with LAMA (left) and LAMA without action offset (right). The character in original LAMA moves forward while tilting its arms to avoid collision with walls, while in LAMA without action offset does not.

intersection points (Sec. 3.4) goes over a certain threshold.³

- **Naturalness:** We measure the naturalness of the synthesized motions by measuring the Fréchet distance, as reported in [15, 35, 40] between the synthesized motion and motions from motion capture data. Features are extracted from motion sequences and the Fréchet distance is computed with the extracted features. We measure the naturalness of character root movements FD_{root} , including root orientation and velocity, and character joint rotations FD_{joint} .

Baselines. We compare our LAMA with the state-of-the-art approaches as well as variations of ours.

- **Wang et al. [60]** is the state-of-the-art long term motion synthesis method for human-scene interactions within a given 3D scene. We use the author’s code for evaluation. As Wang et al. uses optimization to post-process the synthesized motion to improve foot contact and reduce collisions, we both compare Wang et al. with and without optimization.
- **SAMP [15]** generates interactions which can be generalized not only for object variations but also random starting points within a given 3D scene. SAMP explicitly exploits a path planning module to navigate through cluttered 3D environments.
- **Ablative baselines** We perform ablation studies on the action controller and task-adaptive motion editing module. We perform ablation studies on the scene reward r_{coli} , and action offset a_t^{offset} to present the contribution of both terms on our system’s capability to generate scene-aware motions. We also compare our method without the transition reward $r_{\Delta t}$ and $r_{\Delta v}$ terms (Sec. 3.4) in the action controller. Finally, we demonstrate the strength of our task-adaptive motion editing module to edit motions naturally (Sec. 3.5) by comparing with inverse kinematics (IK).

4.2. Comparisons with Previous Work

Quantitative Evaluation. We compare methods in 6 different scenarios from various 3D scenes in the PROX dataset [16]. Foot contact is automatically labeled based on

positional velocity of the foot joint. Foot slip metric is measured by foot joint positions. To compute penetration metric in a fair way, SMPL-X outputs of Wang et al. and SAMP are converted to box-shaped skeletons as in ours and intersection point are counted. Table 1 shows the results.

As shown, our LAMA outperforms Wang et al both in naturalness and physical plausibility. It is noted that Wang et al performs optimization as post-processing to explicitly minimize foot slip, and yet LAMA still shows on-par performance against it (and better in all other metrics). Compared with SAMP, our method shows much better results in plausibility metrics (both Slip and Penetration), and shows slightly better performance in naturalness. Apart from SAMP which relies on a separate navigation module, our RL-based action controller handles collisions in the same way of scene-interaction and shows much better performance in in complex and cluttered 3D scenes.

A Human Study. To further validate our results, we compare the quality of our output over other baselines, Wang et al. and SAMP, through A/B testing from human observers. For the study, we choose 5 scenarios from different indoor scenes, and render the results of each method using the exactly same view and 3D characters, so that they cannot be distinguished from the appearance side. We build two separate sets, where in each set the result videos of our method are shown with each competitor side by side in a random order. Human observers are asked to choose a motion clip that is more human-like and plausible in the given 3D scene. We perform each set of tests with non-overlapping 15 participants. See our supp. mat. for more details about the study setup. As the result, the outputs of our method are preferred by the majority (more than 50% voting) in all cases. By considering all votes independently, our method are preferred **80.0%** over SAMP and **97.3%** over Wang et al.’s work. In particular, we found that our method greatly outperform the competing methods in terms of the naturalism of foot stepping, transition between locomotion and action, and collision avoidance with the scenes. See our supp. videos for more results.

³10 for legs and 7 for arms

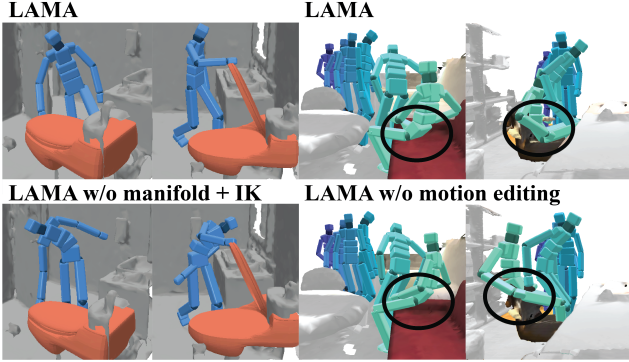


Figure 8. (a) Comparison with LAMA (top) and LAMA without manifold and replaced with IK (bottom) of a character opening the toilet lid. (b) Comparison with LAMA (top) and LAMA without motion editing (bottom) in sitting.

4.3. Ablation Studies

Ablation Studies on Action Controller. We quantitatively compare the original LAMA and the LAMA without collision reward r_{coli} . We intend to demonstrate the role of r_{coli} that enforces the action controller to search for optimal actions for generating motions without collisions. Ablation studies are done in 5 PROX scenes. In the original LAMA, penetrations occur in only **1.1%** of the frames among the whole motion sequences, while the ratio is **15.7%** in LAMA without collision reward. The result supports that the collision reward r_{coli} enforces the action controller to compute optimal actions for synthesizing body movement according to the spatial constraint of the given 3D scene. Example results are shown in Fig. 6.

We also compare the contribution of other components in the action controller module in generating natural interactions. As seen in Fig. 7, with the action controller without \mathbf{a}_t^{offset} the character fails to avoid penetration with objects or walls, as the raw motion from the motion database does not have any information of the scene. This demonstrates that action offset also plays a role in generating detailed scene-aware poses even from raw motion capture data. Moreover, the results with the action controller without smoothness rewards $r_{\Delta t}$ and $r_{\Delta v}$ are not smooth enough, showing unnatural movements such as jerking. These ablation studies justify the advantages of our reward terms.

Ablation Studies on Task-Adaptive Motion Editing. We ablate our motion editing module by replacing it with an alternative approach via Inverse-Kinematics (IK). An example result is shown in Fig. 8 (left). For manipulation, the results with IK show jerky and awkward motions because the temporal and inter-joint correlations in natural human motions are not reflected in IK, while original LAMA with task-adaptive motion editing module shows much natural motions. Our motion editing module can also be used to

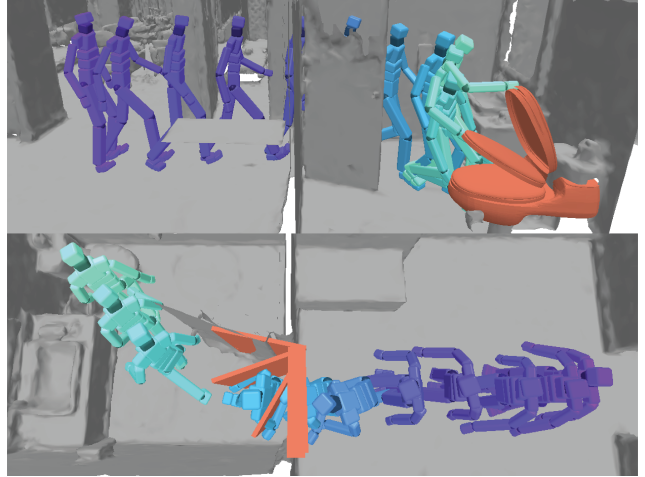


Figure 9. Examples of synthesized manipulation motions. The target object for manipulation is colored as orange. Top is a motion sequence of walking and opening a toilet lid, and the bottom is a sequence of walking and opening doors. The character is colored purple at start and aqua at the end.

further adjust the character movements in different object geometries, going over the limit of the motion database. As seen in Fig 8 (right), the motion editing module enables the character to properly sit in chairs with various sizes.

5. Discussion

In this paper, we present a method to synthesize locomotion, scene-interaction, and manipulation in a unified system. Leveraging a RL framework with motion matching, our method enables to produce natural and plausible humans motions in complex and cluttered 3D environments only with a limited amount of motion-only datasets. Our method has been thoroughly evaluated in diverse scenarios, outperforming previous approaches [15, 60]. We also demonstrate the robustness and generalization ability of our system by covering a wide range of human interactions in many different 3D environments.

While our RL-based method can be generalized to any unseen 3D environments, a new control policy has to be trained for each motion sequence. Combining RL with a supervised learning framework for better efficiency can be an interesting future research direction. Furthermore, although we assume a fixed skeletal information throughout the system, interaction motions may change depending on the character’s body shape and sizes. We leave synthesizing motions on varying body shapes as future work.

Acknowledgments: This work was supported by SNU-Naver Hyperscale AI Center, SNU Creative-Pioneering Researchers Program, and NRF grant funded by the Korea government (MSIT) (No. 2022R1A2C209272411).

A. Supplementary Video

The supplementary video shows the results of our method, LAMA, on various scenarios. In the video, we show the human motion synthesis results on PROX [16], Matterport3D [7], and also our own home-brewed 3D scene produced by Polycam App [1] in an iPad pro. We use SAPIEN [63] object meshes for manipulation examples. As shown, our method successfully produces plausible and natural human motions in many challenging scenarios. Our supplementary video contains several ablation studies of our method by showing the importance of collision reward r_{coli} in Eq. (4), transition reward ($r_{\Delta t}$, $r_{\Delta v}$) in Eq. (8), posture offset $\mathbf{a}_t^{\text{offset}}$ in Action Controller (Sec. 3.2), and our motion editing modules (Sec. 3.5) compared to the traditional Inverse Kinematics (IK). We also show the comparison with previous state-of-the arts [15, 59, 60] and demonstrate that our results produces better quality of motions with better collision avoidance performance in complicated 3D scenes.

B. Additional Details on Implementations

B.1. Action Controller

Implementation Details. For the action controller **A** and motion synthesizer module **S**, we use the animation library DART [27]. We also use a publicly available PPO implementation [32, 41], where we remove the variable time-stepping functions stepping in [32] by following the original PPO algorithm. The details of the training regarding the policy and value network of the action controller are written in Table 2.

Early Termination Conditions. As written in the main paper, the episode is terminated (1) when the character moves out of the scene bounding box; (2) when the collision reward r_{coli} is under a certain threshold; or (3) when the root of the human character is located in the blocked (occupied) regions of the scenes in 2D grid space during the locomotion status.

Name	Value
Learning rate of policy network	2e-4
Learning rate of value network	0.001
Discount factor (γ)	0.95
GAE and TD (λ)	0.95
Clip parameter (ϵ)	0.2
# of tuples per policy update	30000
Batch size for policy/value update	512

Table 2. Details on the hyper-parameters for learning the control policy of the action controller **A**.

B.2. Motion Synthesizer

Motion Database Information. As described in our main paper, we pre-process the motion segments by selectively collecting and clipping from Ubisoft La Forge [14], COUCH [70], and SAMP [15]. The length (in frames) of motion segments (“Seg. Length” in tables), number of motion segment (“Seg. Count” in tables), and the number of total frames (“Total Frames” in tables) are summarized in Table 3.

Action-Specific Feature Definition. The motion feature, as defined in our main paper Sec 3.3, represents both the current state of the motion and a short term future movements: $f(\mathbf{m}) = \{\{p_j\}, \{\dot{p}_j\}, \theta_{up}, c, \mathbf{o}_{\text{future}}\}$. In particular the action specific feature $\mathbf{o}_{\text{future}} = \{\{p_0^{dt}\}, \{r_0^{dt}\}\}$ contains future motions so that the motion search process can take into account the future motion consistency, where $p_0^{dt}, r_0^{dt} \in \mathbb{R}^2$ are the position and orientation of root joint at dt frames later from the current target frame. For locomotion, we extract $dt = 10, 20$, and 30 frames in the future (at 30Hz) following [9], as addressed in our main paper. For sitting, we specifically choose dt as the frame where the character completes the sit-down motion. The major motivation of this design choice is encourage the motion synthesizer to search the motion clips with the desired target action.

Computation Cost for Searching. The computation time for searching the motion database is done between 1-2 milliseconds in CPU, where we test on AMD Ryzen 5950X CPU. The number of search times varies and is dependent to the 3D scenes and desired motions. In one of our scenarios, total 17 searches in locomotion(walk) and 14 in action(sit) were done. For locomotion, the searching time is average 1.743 milliseconds (standard deviation 0.46) and for action(sit) 1.103 milliseconds (standard deviation 0.63).

B.3. Motion Editing via Motion Manifold

Implementation Details. For the convolutional autoencoder of task-adaptive motion editing, we use PyTorch [42], FairMotion [12], and PyTorch3d [48]. The autoencoder is trained with the Adam optimizer with learning rate 0.0001. We use 3 layers of 1D temporal-convolutions with kernel width of 25 and stride 2, and the channel dimension of each output feature is 256. The training datasets are summarized in Table 4. Note that we use different pre-processing steps between Motion editing module and Motion Synthesizer.

Reconstruction Loss. The encoder Ψ and decoder Ψ^{-1} are trained based on reconstruction loss $\mathcal{L}_{\text{recon}} = \|\mathbf{X} - \Psi^{-1}(\Psi(\mathbf{X}))\|^2$, where:

$$\mathcal{L}_{\text{recon}} = w_c \mathcal{L}_{\text{contact}} + w_r \mathcal{L}_{\text{root}} + w_q \mathcal{L}_{\text{quat}} + w_p \mathcal{L}_{\text{pos}}. \quad (9)$$

$\mathcal{L}_{\text{contact}}$, $\mathcal{L}_{\text{root}}$, and $\mathcal{L}_{\text{quat}}$ are the MSE losses of foot contact labels, root status (height and transform relative to the previous frame projected on the XZ plane), and the joint rotations in 6D representations [73]. To penalize errors accumulating along the kinematic chain, we perform forward kinematics (FK) and measure the global position distance of joints between original and reconstructed motion. As global positions of the joints are highly dependent on the root positions, for the early epochs, the distance is measured based on root-centric coordinates to ignore the global location of roots, which we found empirically more stable.

Motion Editing Loss For motion editing, the positional loss and regularization loss are defined as follows.

$$\begin{aligned} \mathcal{L} &= w_p \mathcal{L}_{\text{pos}} + w_f \mathcal{L}_{\text{foot}} + w_r \mathcal{L}_{\text{root}}, \quad \text{where} \\ \mathcal{L}_{\text{pos}} &= \sum_{j, \mathbf{q}_j \in \phi} \|\mathbf{p}_j - \mathbf{q}_j\|^2, \quad \text{if } \phi \text{ exists at } t \\ \mathcal{L}_{\text{foot}} &= \sum_{\text{foot}} \|\mathbf{p}_{\text{foot}}^e - \mathbf{p}_{\text{foot}}^i\|^2, \\ \mathcal{L}_{\text{root}} &= w_r \|\mathbf{r}_{\text{xz}}^e - \mathbf{r}_{\text{xz}}^i\|^2 + w_{\Delta r} \|\dot{\mathbf{r}}_{\text{xz}}^e - \dot{\mathbf{r}}_{\text{xz}}^i\|^2. \end{aligned} \quad (10)$$

\mathbf{p}_j denotes positions of joint j , and \mathbf{r} , $\dot{\mathbf{r}}$ denotes root positions and velocities respectively. Superscript e and i indicates whether it is from edited or initial motion, respectively. Subscript xz indicates the vector is projected onto the XZ plane. The loss term \mathcal{L} enforces the edited motion to maintain contact and root trajectory (in the XZ plane) of the initial motion, while generating natural movements of the other joints to meet the sparse positional constraints.

Generating Interaction Cue for Manipulation To synthesize character’s arm motions naturally interacting with the movements of articulated target objects, we produce desired interaction cues by producing the 3D trajectories of a chosen 3D position of the object at which the hand part of the character are expected to touch. Specifically, we apply the expected articulated motion of the 3D object model to produce the 3D trajectory of a chosen object vertex, $\mathbf{v}(R_t, T_t, \theta_t)$, where R_t, T_t are the global orientation and translation of the object and θ_t is the parameters for the object articulation (e.g., the hinge angle of the cover of a laptop) at time t . $v(\cdot)$ represents the 3D location of the chosen vertex v . To this end, we input the produced trajectory as the desired 3D interaction cue for a character’s joint (e.g., a hand joint) assuming the joint is touching this object trajectory for manipulation $\phi = [\mathbf{v}(R_t, T_t, \theta_t)]_t$. Note that, in our visualization, we apply the desired articulated motions for the 3D object at each time, synced to the produced interaction cues.

Label	Seg. Length	Seg. Count	Total Frames
Locomotion	10	11063	11498
Sit	50 – 85	5842	14942

Table 3. Details on pre-processed motion datasets per each action category for training our motion synthesizer **S**.

Name	Value
Motion sequence length	120
Number of sequence (training)	11397
Number of sequence (validation)	3135
Number of sequence (test)	2139

Table 4. Details on pre-processed motion datasets for training our motion editing module **M**.

C. More Details on Experiments

C.1. Frechet Distance Features

FD_{root} is computed by root feature vector, which is a concatenated vector of root orientation in angle-axis representation, root up vector, and root transform relative to the previous frame. We note that all of the motions for comparison have the same up axis (y) and floor plane (xz). FD_{joint} is computed by joint feature vector, represented as joint orientations in angle-axis representation, excluding the root.

References

- [1] Polycam - lidar and 3d scanner for iphone & android. <https://poly.cam/>. 9
- [2] Kfir Aberman, Peizhuo Li, Dani Lischinski, Olga Sorkine-Hornung, Daniel Cohen-Or, and Baoquan Chen. Skeleton-aware networks for deep motion retargeting. *ACM Trans. Graph.*, 39(4), 2020. 3
- [3] Kfir Aberman, Yijia Weng, Dani Lischinski, Daniel Cohen-Or, and Baoquan Chen. Unpaired motion style transfer from video to animation. *ACM Trans. Graph.*, 39(4), 2020. 3
- [4] Kevin Bergamin, Simon Clavet, Daniel Holden, and James Richard Forbes. Drecon: data-driven responsive control of physics-based characters. *ACM Trans. Graph.*, 38(6), 2019. 3
- [5] Michael Büttner and Simon Clavet. Motion matching - the road to next gen animation. In *Proc. of Nucl.ai*, 2015. 2, 4
- [6] Zhe Cao, Hang Gao, Kartikeya Mangalam, Qi-Zhi Cai, Minh Vo, and Jitendra Malik. Long-term human motion prediction with scene context. In *ECCV*, 2020. 2
- [7] Angel Chang, Angela Dai, Thomas Funkhouser, Maciej Halber, Matthias Niessner, Manolis Savva, Shuran Song, Andy Zeng, and Yinda Zhang. Matterport3d: Learning from rgb-d data in indoor environments. In *3DV*, 2017. 6, 9
- [8] Yu-Wei Chao, Jimei Yang, Weifeng Chen, and Jia Deng. Learning to sit: Synthesizing human-chair interactions via hierarchical control. In *AAAI*, 2021. 2

- [9] Simon Clavet. Motion matching and the road to next-gen animation. In *Proc. of GDC*, 2016. 2, 4, 9
- [10] Haegwang Eom, Daseong Han, Joseph S Shin, and Junyong Noh. Model predictive control with a visuomotor system for physics-based character animation. *ACM Trans. Graph.*, 39(1), 2019. 1, 2
- [11] Katerina Fragkiadaki, Sergey Levine, Panna Felsen, and Jitendra Malik. Recurrent network models for human dynamics. In *ICCV*, 2015. 2
- [12] Deepak Gopinath and Jungdam Won. fairmotion - tools to load, process and visualize motion capture data. Github, 2020. 9
- [13] Ikhsanul Habibie, Daniel Holden, Jonathan Schwarz, Joe Yearsley, and Taku Komura. A recurrent variational autoencoder for human motion synthesis. In *BMVC*, 2017. 2
- [14] Félix G Harvey, Mike Yurick, Derek Nowrouzezahrai, and Christopher Pal. Robust motion in-betweening. *ACM Trans. Graph.*, 39(4), 2020. 3, 6, 9
- [15] Mohamed Hassan, Duygu Ceylan, Ruben Villegas, Jun Saito, Jimei Yang, Yi Zhou, and Michael Black. Stochastic scene-aware motion prediction. In *ICCV*, 2021. 1, 2, 3, 6, 7, 8, 9
- [16] Mohamed Hassan, Vasileios Choutas, Dimitrios Tzionas, and Michael J. Black. Resolving 3D human pose ambiguities with 3D scene constraints. In *ICCV*, 2019. 2, 6, 7, 9
- [17] Mohamed Hassan, Partha Ghosh, Joachim Tesch, Dimitrios Tzionas, and Michael J Black. Populating 3d scenes by learning human-scene interaction. In *CVPR*, 2021. 1, 2
- [18] Daniel Holden, Oussama Kanoun, Maksym Perepichka, and Tiberiu Popa. Learned motion matching. *ACM Trans. Graph.*, 39(4), 2020. 4
- [19] Daniel Holden, Taku Komura, and Jun Saito. Phase-functioned neural networks for character control. *ACM Trans. Graph.*, 36(4), 2017. 3
- [20] Daniel Holden, Jun Saito, and Taku Komura. A deep learning framework for character motion synthesis and editing. *ACM Trans. Graph.*, 35(4), 2016. 2, 3, 6
- [21] Chun-Hao P Huang, Hongwei Yi, Markus Höschle, Matvey Safroshkin, Tsvetelina Alexiadis, Senya Polikovsky, Daniel Scharstein, and Michael J Black. Capturing and inferring dense full-body human-scene contact. In *CVPR*, 2022. 2
- [22] Kyunglyul Hyun, Kyungho Lee, and Jehee Lee. Motion grammars for character animation. In *Computer Graphics Forum*, volume 35, 2016. 2
- [23] Yuheng Jiang, Suyi Jiang, Guoxing Sun, Zhuo Su, Kaiwen Guo, Minye Wu, Jingyi Yu, and Lan Xu. Neuralhofusion: Neural volumetric rendering under human-object interactions. In *CVPR*, 2022. 2
- [24] Vladimir G Kim, Siddhartha Chaudhuri, Leonidas Guibas, and Thomas Funkhouser. Shape2pose: Human-centric shape analysis. *ACM Trans. Graph.*, 33(4), 2014. 1, 2
- [25] Diederik P Kingma and Jimmy Ba. Adam: A method for stochastic optimization. *arXiv preprint arXiv:1412.6980*, 2014. 6
- [26] Jehee Lee, Jinxiang Chai, Paul SA Reitsma, Jessica K Hodgins, and Nancy S Pollard. Interactive control of avatars animated with human motion data. In *Proceedings of the 29th annual conference on Computer graphics and interactive techniques*, 2002. 2
- [27] Jeongseok Lee, Michael X Grey, Sehoon Ha, Tobias Kunz, Sumit Jain, Yuting Ye, Siddhartha S Srinivasa, Mike Stilman, and C Karen Liu. Dart: Dynamic animation and robotics toolkit. *The Journal of Open Source Software*, 3(22), 2018. 9
- [28] Jehee Lee and Kang Hoon Lee. Precomputing avatar behavior from human motion data. In *Proceedings of the 2004 ACM SIGGRAPH/Eurographics symposium on Computer animation*, 2004. 3
- [29] Kyungho Lee, Seyoung Lee, and Jehee Lee. Interactive character animation by learning multi-objective control. *ACM Trans. Graph.*, 37(6), 2018. 3
- [30] Kyungho Lee, Sehee Min, Sunmin Lee, and Jehee Lee. Learning time-critical responses for interactive character control. *ACM Trans. Graph.*, 40(4), 2021. 3
- [31] Kang Hoon Lee, Myung Geol Choi, and Jehee Lee. Motion patches: building blocks for virtual environments annotated with motion data. In *ACM SIGGRAPH 2006 Papers*. 2006. 2
- [32] Seyoung Lee, Sunmin Lee, Yongwoo Lee, and Jehee Lee. Learning a family of motor skills from a single motion clip. *ACM Trans. Graph.*, 40(4), 2021. 3, 9
- [33] Seunghwan Lee, Moonseok Park, Kyoungmin Lee, and Jehee Lee. Scalable muscle-actuated human simulation and control. *ACM Trans. Graph.*, 38(4), 2019. 5
- [34] Sergey Levine, Jack M Wang, Alexis Haraux, Zoran Popović, and Vladlen Koltun. Continuous character control with low-dimensional embeddings. *ACM Trans. Graph.*, 31(4), 2012. 3
- [35] Ruilong Li, Shan Yang, David A. Ross, and Angjoo Kanazawa. Ai choreographer: Music conditioned 3d dance generation with aist++. In *ICCV*, 2021. 2, 7
- [36] Hung Yu Ling, Fabio Zinno, George Cheng, and Michiel Van De Panne. Character controllers using motion vaes. *ACM Trans. Graph.*, 39(4), 2020. 3
- [37] Kovar Lucas, Gleicher Michael, and Pighin Frédéric. Motion graphs. In *Proceedings of the 29th Annual Conference on Computer Graphics and Interactive Techniques*, 2002. 2
- [38] Julieta Martinez, Michael J Black, and Javier Romero. On human motion prediction using recurrent neural networks. In *CVPR*, 2017. 2
- [39] Josh Merel, Saran Tunyasuvunakool, Arun Ahuja, Yuval Tassa, Leonard Hasenclever, Vu Pham, Tom Erez, Greg Wayne, and Nicolas Heess. Catch & carry: reusable neural controllers for vision-guided whole-body tasks. *ACM Trans. Graph.*, 39(4), 2020. 2
- [40] Evonne Ng, Hanbyul Joo, Liwen Hu, Hao Li, , Trevor Darrell, Angjoo Kanazawa, and Shiry Ginosar. Learning to listen: Modeling non-deterministic dyadic facial motion. In *CVPR*, 2022. 7
- [41] Soohwan Park, Hoseok Ryu, Seyoung Lee, Sunmin Lee, and Jehee Lee. Learning predict-and-simulate policies from unorganized human motion data. *ACM Trans. Graph.*, 38(6), 2019. 3, 5, 9

- [42] Adam Paszke, Sam Gross, Francisco Massa, Adam Lerer, James Bradbury, Gregory Chanan, Trevor Killeen, Zeming Lin, Natalia Gimelshein, Luca Antiga, Alban Desmaison, Andreas Kopf, Edward Yang, Zachary DeVito, Martin Raison, Alykhan Tejani, Sasank Chilamkurthy, Benoit Steiner, Lu Fang, Junjie Bai, and Soumith Chintala. Pytorch: An imperative style, high-performance deep learning library. In *Advances in Neural Information Processing Systems 32*, pages 8024–8035. Curran Associates, Inc., 2019. 9
- [43] Xue Bin Peng, Pieter Abbeel, Sergey Levine, and Michiel Van de Panne. Deepmimic: Example-guided deep reinforcement learning of physics-based character skills. *ACM Trans. Graph.*, 37(4), 2018. 3, 5
- [44] Xue Bin Peng, Yunrong Guo, Lina Halper, Sergey Levine, and Sanja Fidler. Ase: Large-scale reusable adversarial skill embeddings for physically simulated characters. *ACM Trans. Graph.*, 41(4), 2022. 3
- [45] Xue Bin Peng, Ze Ma, Pieter Abbeel, Sergey Levine, and Angjoo Kanazawa. Amp: Adversarial motion priors for stylized physics-based character control. *ACM Trans. Graph.*, 40(4), 2021. 3
- [46] Mathis Petrovich, Michael J Black, and Gül Varol. Action-conditioned 3d human motion synthesis with transformer vae. In *ICCV*, 2021. 2, 3
- [47] Yuzhe Qin, Yueh-Hua Wu, Shaowei Liu, Hanwen Jiang, Ruihan Yang, Yang Fu, and Xiaolong Wang. Dexmv: Imitation learning for dexterous manipulation from human videos. In *ECCV*, 2022. 1, 2
- [48] Nikhila Ravi, Jeremy Reizenstein, David Novotny, Taylor Gordon, Wan-Yen Lo, Justin Johnson, and Georgia Gkioxari. Accelerating 3d deep learning with pytorch3d. *arXiv:2007.08501*, 2020. 9
- [49] Manolis Savva, Angel X Chang, Pat Hanrahan, Matthew Fisher, and Matthias Nießner. Pigraphs: learning interaction snapshots from observations. *ACM Trans. Graph.*, 35(4), 2016. 1, 2
- [50] John Schulman, Filip Wolski, Prafulla Dhariwal, Alec Radford, and Oleg Klimov. Proximal policy optimization algorithms. *arXiv preprint arXiv:1707.06347*, 2017. 5
- [51] Hubert PH Shum, Taku Komura, Masashi Shiraishi, and Shuntaro Yamazaki. Interaction patches for multi-character animation. *ACM Trans. Graph.*, 27(5), 2008. 2
- [52] Sebastian Starke, Ian Mason, and Taku Komura. Deepphase: periodic autoencoders for learning motion phase manifolds. *ACM Trans. Graph.*, 41(4):1–13, 2022. 3
- [53] Sebastian Starke, He Zhang, Taku Komura, and Jun Saito. Neural state machine for character-scene interactions. *ACM Trans. Graph.*, 38(6), 2019. 1, 2
- [54] Omid Taheri, Vasileios Choutas, Michael J Black, and Dimitrios Tzionas. Goal: Generating 4d whole-body motion for hand-object grasping. In *CVPR*, 2022. 1, 2
- [55] Omid Taheri, Nima Ghorbani, Michael J Black, and Dimitrios Tzionas. Grab: A dataset of whole-body human grasping of objects. In *ECCV*, 2020. 1, 2
- [56] Graham W Taylor and Geoffrey E Hinton. Factored conditional restricted boltzmann machines for modeling motion style. In *ICML*, 2009. 2
- [57] Adrien Treuille, Yongjoon Lee, and Zoran Popović. Near-optimal character animation with continuous control. In *ACM SIGGRAPH 2007 papers*. 2007. 3
- [58] Ruben Villegas, Jimei Yang, Yuliang Zou, Sungryull Sohn, Xunyu Lin, and Honglak Lee. Learning to generate long-term future via hierarchical prediction. In *ICML*, 2017. 2
- [59] Jingbo Wang, Yu Rong, Jingyuan Liu, Sijie Yan, Dahua Lin, and Bo Dai. Towards diverse and natural scene-aware 3d human motion synthesis. In *CVPR*, 2022. 1, 2, 3, 9
- [60] Jiashun Wang, Huazhe Xu, Jingwei Xu, Sifei Liu, and Xiaolong Wang. Synthesizing long-term 3d human motion and interaction in 3d scenes. In *CVPR*, 2021. 1, 2, 6, 7, 8, 9
- [61] Jingbo Wang, Sijie Yan, Bo Dai, and Dahua Lin. Scene-aware generative network for human motion synthesis. In *CVPR*, 2021. 2
- [62] Jungdam Won, Deepak Gopinath, and Jessica Hodgins. A scalable approach to control diverse behaviors for physically simulated characters. *ACM Trans. Graph.*, 39(4), 2020. 3
- [63] Fanbo Xiang, Yuzhe Qin, Kaichun Mo, Yikuan Xia, Hao Zhu, Fangchen Liu, Minghua Liu, Hanxiao Jiang, Yifu Yuan, He Wang, et al. Sapien: A simulated part-based interactive environment. In *CVPR*, 2020. 6, 9
- [64] Xianghui Xie, Bharat Lal Bhatnagar, and Gerard Pons-Moll. Chore: Contact, human and object reconstruction from a single rgb image. In *ECCV*, 2022. 1, 2
- [65] Xiang Xu, Hanbyul Joo, Greg Mori, and Manolis Savva. D3d-hoi: Dynamic 3d human-object interactions from videos. *arXiv preprint arXiv:2108.08420*, 2021. 2
- [66] Zeshi Yang, Kangkang Yin, and Libin Liu. Learning to use chopsticks in diverse gripping styles. *ACM Trans. Graph.*, 41(4), 2022. 1, 2
- [67] He Zhang, Yuting Ye, Takaaki Shiratori, and Taku Komura. Manipnet: Neural manipulation synthesis with a hand-object spatial representation. *ACM Trans. Graph.*, 40(4), 2021. 1, 2
- [68] Jason Y. Zhang, Sam Pepose, Hanbyul Joo, Deva Ramanan, Jitendra Malik, and Angjoo Kanazawa. Perceiving 3d human-object spatial arrangements from a single image in the wild. In *ECCV*, 2020. 2
- [69] Siwei Zhang, Yan Zhang, Qianli Ma, Michael J Black, and Siyu Tang. Place: Proximity learning of articulation and contact in 3d environments. In *3DV*, 2020. 1, 2
- [70] Xiaohan Zhang, Bharat Lal Bhatnagar, Sebastian Starke, Vladimir Guzov, and Gerard Pons-Moll. Couch: Towards controllable human-chair interactions. In *ECCV*, 2022. 1, 2, 6, 9
- [71] Yan Zhang, Mohamed Hassan, Heiko Neumann, Michael J Black, and Siyu Tang. Generating 3d people in scenes without people. In *CVPR*, 2020. 1, 2
- [72] Kaifeng Zhao, Shaofei Wang, Yan Zhang, Thabo Beeler, and Siyu Tang. Compositional human-scene interaction synthesis with semantic control. In *ECCV*, 2022. 1, 2
- [73] Yi Zhou, Connelly Barnes, Lu Jingwan, Yang Jimei, and Li Hao. On the continuity of rotation representations in neural networks. In *CVPR*, 2019. 4, 6, 10